

Hexanuclear Ferric Complexes Possessing Different Degrees of Spin Frustration

Cheryl A. Christmas,¹ Hui-Lien Tsai,¹ Luca Pardi,² Janet M. Kesselman,¹ Peter K. Gantzel,¹ Raj K. Chadha,¹ Dante Gatteschi,^{*,2} Daniel F. Harvey,^{*,1} and David N. Hendrickson^{*,1}

Contribution from the Department of Chemistry-0506, University of California at San Diego, La Jolla, California 92093-0506, and the Dipartimento di Chimica, Università di Firenze, 50144 Firenze, Italy

Received June 24, 1993*

Abstract: The synthesis, single-crystal X-ray structures, and magnetochemical properties are reported for two new hexanuclear ferric complexes, $[\text{Fe}_6(\mu_3\text{-O})_2(\mu_2\text{-OH})_2(\mu_2\text{-O}_2\text{CCH}_3)_{10}(\text{C}_7\text{H}_{11}\text{N}_2\text{O})_2] \cdot 4\text{CH}_2\text{Cl}_2$ (**9**·4CH₂Cl₂) and $[\text{Fe}_6(\mu_3\text{-O})_2(\text{C}_6\text{H}_6\text{NO})_8\text{Cl}_4](\text{ClO}_4)_2 \cdot 4\text{MeCN}$ (**10**·4MeCN). The ligand $\text{C}_7\text{H}_{11}\text{N}_2\text{O}^-$ is the anion of 2-(*N*-methylimidazol-2-yl)-2-hydroxypropane and $\text{C}_6\text{H}_6\text{NO}^-$ is the anion of 2-pyrididylcarbinol. The reaction of $[\text{Fe}_3\text{O}(\text{OAc})_6(\text{py})_3]\text{ClO}_4$ in acetonitrile with 2-(*N*-methylimidazol-2-yl)-2-hydroxypropane gives a brown oil which can be crystallized via vapor diffusion of CH_2Cl_2 with hexanes to give complex **9**·4CH₂Cl₂. The reaction of $\text{FeCl}_3 \cdot 6\text{H}_2\text{O}$ and 2-pyridylcarbinol in acetonitrile gives, upon addition of NaClO_4 , complex **10**·4MeCN. Complex **9** has six high-spin Fe^{III} ions and can be viewed as two trinuclear μ_3 -oxo-bridged subunits bridged by two μ_2 -hydroxo and μ_2 -acetato ligands. Complex **10** can also be viewed as two asymmetric triangular Fe_3 - μ_3 -oxo subunits bridged together by alkoxo groups. However, in complex **9** there is a planar array of six Fe^{III} ions, whereas in complex **10** the six high-spin Fe^{III} ions are arranged in a chair conformation. Variable temperature DC magnetic susceptibility data measured at 10.0 kG are presented for both complexes. For complex **9**·3/2CH₂Cl₂ μ_{eff} /molecule was found to be 9.10 μ_{B} at 300.0 K, and as the temperature is decreased, this value increases to a maximum of 10.55 μ_{B} at 30.0 K, whereupon there is a decrease to 9.77 μ_{B} at 5.00 K. Complex **10**·MeCN in a 10.0 kG field gives μ_{eff} /molecule = 8.82 μ_{B} at 320.0 K. In contrast to **9**, the μ_{eff} /molecule for complex **10**·MeCN decreases with decreasing temperature to 6.08 μ_{B} at 5.01 K. Least-squares fitting of the reduced magnetization ($M/N\mu_{\text{B}}$) versus H/T data for paraffin-embedded complex **9**·3/2CH₂Cl₂ in the range of 5.00–50.0 kG external field and 2.0–30.0 K clearly shows that complex **9** has a well isolated $S_{\text{T}} = 5$ ground state. Reduced magnetization versus H/T data are also presented for a paraffin-embedded sample of complex **10**·MeCN in external fields of 0.50–50 kG at temperatures of 2–30 K. Fitting the high-field data suggests the presence of a $S_{\text{T}} = 3$ ground state. However, the fit of the low-field data is not good for just an isolated $S_{\text{T}} = 3$ ground state. Theoretical calculations were carried out for two of the known Fe^{III}_6 complexes. The energies of all of the 4332 different spin states of a Fe^{III}_6 complex were calculated, taking into account the pairwise magnetic exchange interactions within μ_3 -oxo-bridged Fe^{III}_3 triangular subunits (parameters J_1 , J_2 , and J_3) and the interaction (J_4) between iron ions in two Fe_3O triangular subunits. The 20–320 K data measured at 10.0 kG for complex **5** (isostructural to **9**) could be fit well with a theoretical calculation where $J_1 = -5.6(5) \text{ cm}^{-1}$, $J_2 = J_3 = -38(1) \text{ cm}^{-1}$, and $J_4 = -7.5(1) \text{ cm}^{-1}$. In agreement with experimental data, a well-isolated $S_{\text{T}} = 5$ ground state is predicted. The theoretical fit of 20–320 K data for complex **10**·MeCN in a 10.0 kG field gives fitting parameters of $J_1 = J_2 = -18(1) \text{ cm}^{-1}$, $J_3 = -52(2) \text{ cm}^{-1}$, and $J_4 = -3(2) \text{ cm}^{-1}$. Even though all pairwise exchange interactions are antiferromagnetic, a Fe^{III}_6 complex can have a ground state with a spin ranging from $S_{\text{T}} = 0$ to 5. The ground state found for a given Fe^{III} complex is dependent upon which pairwise antiferromagnetic interactions are strongest.

Introduction

Polynuclear iron complexes are being studied for at least three different reasons. First, it is important to understand the iron storage protein ferritin which is involved in the storage, detoxification, and recycling of iron.³ Polymetal oxo-hydroxo complexes of variable size are also being studied in order to understand the factors that control when a complex becomes large enough to exhibit properties of single-domain metal oxide particles.⁴ Finally, new polynuclear iron oxo-hydroxo complexes are being prepared in an effort to identify molecules which have a large number of unpaired electrons. These molecules might be useful as building blocks for molecular-based magnetic materials.

Magnetite (Fe_3O_4) and hematite ($\alpha\text{-Fe}_2\text{O}_3$) are obviously important magnetic oxides.⁵ Since the preparation of molecules with large numbers of unpaired electrons is being pursued in many laboratories^{4,6} as a means of obtaining building blocks for molecular-based magnetic materials, polynuclear oxo-hydroxo iron complexes which possess appreciable numbers of unpaired electrons are desirable. The incorporation of spin frustration⁷ into polynuclear oxo-hydroxo iron complexes may be the means to obtain iron complexes with appreciable numbers of unpaired electrons. Spin frustration refers to the situation in a paramagnetic polynuclear complex where the topology of the complex makes it such that the lowest-spin state is not found to be the ground

* Abstract published in *Advance ACS Abstracts*, December 1, 1993.

(1) University of California at San Diego.

(2) Università di Firenze.

(3) (a) Thell, E. C. *Annu. Rev. Biochem.* **1987**, *56*, 289 and references therein. Xu, B.; Chasteen, D. *J. Biol. Chem.* **1991**, *266*, 19965.

(4) (a) Papaefthymiou, G. C. *Phys. Rev.* **1992**, *B46*, 10366. (b) Sessoli, R.; Tsai, H.-L.; Schake, A. R.; Wang, S.; Vincent, J. B.; Folting, K.; Gatteschi, D.; Christou, G.; Hendrickson, D. N. *J. Am. Chem. Soc.* **1993**, *115*, 1804. (c) Caneschi, A.; Gatteschi, D.; Sessoli, R.; Barra, A. L.; Brunel, L. C.; Guillot, M. J. *J. Am. Chem. Soc.* **1991**, *113*, 5873.

(5) *Magnetic Oxides*; Craik, D. J., Ed.; Wiley: New York, 1975; Vols. 1 and 2.

(6) (a) Iwamura, H. *Pure Appl. Chem.* **1987**, *59*, 1595 and references therein. (b) Itoh, K.; Takui, T.; Teki, Y.; Kinoshita, J. *J. Mol. Electron.* **1988**, *4*, 181. (c) Nakamura, N.; Inoue, K.; Iwamura, H.; Fujioka, T.; Sawaki, Y. *J. Am. Chem. Soc.* **1992**, *114*, 1484. (d) Dougherty, D. A. *Pure Appl. Chem.* **1990**, *62*, 519. (e) Caneschi, A.; Gatteschi, D.; Laugier, J.; Rey, P.; Sessoli, R.; Zanchini, C. *J. Am. Chem. Soc.* **1988**, *110*, 2795. (f) Miller, J. S.; Epstein, A. J.; Reiff, W. M. *Chem. Rev.* **1988**, *88*, 201. (g) Kahn, O. *Struct. Bonding (Berlin)* **1987**, *68*, 89.

state, even though all pairwise magnetic exchange interactions are antiferromagnetic. Pairwise interactions between high-spin Fe^{III} are antiferromagnetic; however, with certain molecular topologies spin frustration will lead to complexes with ground states that have several unpaired electrons.⁸

In this paper we will examine the spin frustration that is present in certain Fe^{III}₆ complexes. Eight hexanuclear iron complexes have been previously reported: [Fe₆(μ₃-O)₂(μ₂-OH)₂(μ₂-O₂C(CH₃)₃)₁₂] (1),⁹ [Fe₆(μ₃-O)₂(μ₂-OH)₂(μ₂-O₂CPh)₁₂(OH₂)₂(1,4-dioxane)] (2),¹⁰ [Fe₆(μ₃-O)₂(μ₂-O₂)(μ₂-O₂CPh)₁₂(OH₂)₂] (3),¹¹ [Fe₆(μ₆-O)((OCH₂)₃(CCH₃)₆)₂] (4),¹² [Fe₆(μ₃-O)₂(μ₂-OH)₂(μ₂-O₂CCH₃)₁₀(C₁₀H₁₃N₄O)₂] (5),⁸ [Fe₆(μ₆-O)(μ₂-OCH₃)₁₂(OC H₃)₆] (6),¹³ [Fe₆(μ₄-O)₂(μ₂-OCH₃)₈(OCH₃)₄(tren)₂] (7)¹⁴ (tren = 2,2',2''-triiminotriethylamine), and [Fe₆(μ₃-O)₂(μ₂-OH)₆(ida)₆] (8)¹⁵ (H₂ida = iminodiacetic acid). The preparation and characterization of two new polyoxo hexanuclear Fe^{III} complexes, [Fe₆(μ₃-OH)₂(μ₂-OH)₂(μ₂-O₂CCH₃)₁₀(C₇H₁₁N₂O)₂]·4CH₂Cl₂ (9·4CH₂Cl₂) and [Fe₆(μ₃-O)₂(C₆H₆NO)₈Cl₄](ClO₄)₂·4MeCN (10·4MeCN), are described herein where C₇H₁₁N₂O is the monoanion of 2-(*N*-methylimidazol-2-yl)-2-hydroxypropane and C₆H₆NO is 2-pyridylcarbinol. It will be shown that the spin of the ground state changes from *S* = 0 to 5.

Experimental Section

Physical Measurements. Infrared spectra were collected on a Mattson Galaxy Model 2020 FTIR spectrophotometer as KBr pellets. Electronic absorption spectra were measured with a Hewlett Packard Model 8452A diode array spectrophotometer. DC magnetic susceptibility measurements were carried out on a Quantum Design MPMS SQUID susceptometer. Pascal's constants were used to estimate the diamagnetic correction for the complex, which was then subtracted from the experimental susceptibility to give the molar paramagnetic susceptibility. The computer program GENSPIN¹⁶ was used to analyze variable-field magnetization data.

Preparation of Compounds. All operations were carried out under aerobic conditions at ambient temperature unless otherwise indicated. 2-(*N*-Methylimidazol-2-yl)-2-hydroxypropane¹⁷ and [Fe₃O(OAc)₆(py)₃](ClO₄)₃¹⁸ were prepared as previously described. Acetonitrile (MeCN) was distilled from CaH₂ before use. All remaining solvents and reagents were used as received. Elemental analyses were performed by Galbraith Laboratories, Inc. or Oneida Research Services, Inc. **WARNING:** Though we have encountered no difficulty, appropriate care should be taken during the handling of the potentially explosive perchlorate salts.

(7) (a) Hendrickson, D. N. Spin Frustration in Polynuclear Complexes. In *Research Frontiers in Magnetochemistry*; O'Connor, C. J., Ed.; World Scientific Publishing Co.: London, 1993, in press. (b) McCusker, J. K.; Schmitt, E. A.; Hendrickson, D. N. High Spin Inorganic Clusters: Spin Frustration in Polynuclear Manganese and Iron Complexes. In *Magnetic Molecular Materials*; Gatteschi, D., Kahn, O., Miller, J. S., Palacio, F., Eds.; NATO ASI Series E, No. 198; Kluwer Academic Publishers: Dordrecht, The Netherlands, 1991. (c) Hendrickson, D. N.; Christou, G.; Schmitt, E. A.; Libby, E.; Bashkin, J. S.; Wang, S.; Tsai, H.-L.; Vincent, J. B.; Boyd, P. D. W.; Huffman, J. C.; Foltling, K.; Li, Q.; Streib, W. E. *J. Am. Chem. Soc.* **1992**, *114*, 2455.

(8) (a) McCusker, J. K.; Christmas, C. A.; Hagen, P. M.; Chadha, R. K.; Harvey, D. F.; Hendrickson, D. N. *J. Am. Chem. Soc.* **1991**, *113*, 6114. (b) Harvey, D. F.; Christmas, C. A.; McCusker, J. K.; Hagen, P. M.; Chadha, R. K.; Hendrickson, D. N. *Angew. Chem., Int. Ed. Engl.* **1991**, *30*, 598.

(9) (a) Gérébélou, N. V.; Batsanov, A. S.; Timko, G. A.; Struchkov, Yu. T.; Indrichan, K. M.; Popovich, G. A. *Dokl. Akad. Nauk. SSSR* **1987**, *293*, 364. (b) Batsanov, A. S.; Struchkov, Yu. T.; Timko, G. A. *Koord. Khim.* **1988**, *14*, 266.

(10) Micklitz, W.; Lippard, S. J. *Inorg. Chem.* **1988**, *27*, 3067.

(11) Micklitz, W.; Bott, S. G.; Bentsen, J. G.; Lippard, S. J. *J. Am. Chem. Soc.* **1989**, *111*, 372.

(12) Hergetschweiler, K.; Schmale, H.; Streit, H. M.; Schneider, W. *Inorg. Chem.* **1990**, *29*, 3625.

(13) Hergetschweiler, K.; Schmale, H. W.; Streit, H. M.; Gramlich, V.; Hund, H.-U.; Erni, I. *Inorg. Chem.* **1992**, *31*, 1299.

(14) Nair, V. S.; Hagen, K. S. *Inorg. Chem.* **1992**, *31*, 4048.

(15) Harding, C. J.; Henderson, R. K.; Powell, A. K. *Angew. Chem., Int. Ed. Engl.* **1993**, *32*, 570.

(16) Schmitt, E. A.; Hendrickson, D. N., unpublished results.

(17) Ohta, S.; Matsukawa, M.; Ohashi, N.; Nagayama, K. *Synthesis* **1990**, *78*.

(18) Uemara, S.; Spencer, A.; Wilkinson, G. J. *Chem. Soc., Dalton Trans.* **1973**, 2565.

Table I. Crystallographic Data for [Fe₆O₂(OH)₂(OAc)₁₀(C₇H₁₁N₂O)₂]·4CH₂Cl₂ (9·4 CH₂Cl₂) and [Fe₆O₂(C₆H₆NO)₈Cl₄](ClO₄)₂·4 MeCN (10·4 MeCN)

parameter	9	10
formula	C ₃₈ H ₆₂ N ₄ O ₂₆ Cl ₈ Fe ₆	C ₅₆ H ₆₀ N ₁₂ O ₁₈ Cl ₆ Fe ₆
<i>M_r</i>	1609.6	1737.0
color, habit	brown, prismatic	golden-brown, parallelepiped
cryst dimens, mm	0.22 × 0.25 × 0.42	0.6 × 0.3 × 0.2
cryst system	triclinic	triclinic
space group	<i>P</i> 1̄ (No. 2, <i>C</i> ₁)	<i>P</i> 1̄ (No. 2, <i>C</i> ₁)
temp, K	173	150
cell dimensions		
<i>a</i> , Å	11.384(5)	11.886(5)
<i>b</i> , Å	12.448(4)	13.014(6)
<i>c</i> , Å	12.715(4)	13.081(5)
α, deg	101.31(3)	76.87(3)
β, deg	98.75(3)	83.35(3)
γ, deg	109.01(3)	65.81(3)
<i>V</i> , Å ³	1624.5(10)	1796.9(13)
<i>Z</i> , molecules/cell	1	1
<i>D</i> (calc), g/cm ³	1.645	1.605
abs coeff, mm ⁻¹	1.711	1.476
radiation type	Mo Kα (λ = 0.71073 Å)	Mo Kα (λ = 0.71073 Å)
goodness of fit (<i>S</i>) ^a	2.01	1.45
2θ range, deg	4.0 ≤ 2θ ≤ 45.0	3.0 ≤ 2θ ≤ 50.0
octants collected	± <i>h</i> , ± <i>k</i> , ± <i>l</i>	± <i>h</i> , ± <i>k</i> , ± <i>l</i>
total data	4252	6460
unique data	4252	6341
obsd data	3440, <i>F</i> > 6.0σ(<i>F</i>)	5129, <i>F</i> > 4.0σ(<i>F</i>)
<i>R</i> (<i>F</i>), %	4.06	4.68
<i>wR</i> (<i>wF</i>), %	5.42	6.42

^a *S* = [Σ_{*w*}(|*F*_o - |*F*_c||²)/(*m* - *n*)]^{1/2}. ^b *R* = Σ(|*F*_o - |*F*_c||)/Σ|*F*_o|. ^c *wR* = [(|*F*_o - |*F*_c||²)/Σ|*F*_o|²]^{1/2}. ^d *W*⁻¹ = σ²(*F*) + 0.0004*F*².

[Fe₆O₂(OH)₂(OAc)₁₀(C₇H₁₁N₂O)₂] (9). To a stirred solution of [Fe₃O(OAc)₆(py)₃](ClO₄) (0.238 g, 0.27 mmol) in MeCN (30 mL) was added 2-(*N*-methylimidazol-2-yl)-2-hydroxypropane (0.152 g, 1.09 mmol). After being heated at reflux for 12–16 h, the reaction mixture was concentrated *in vacuo* and the resulting brown oil was crystallized via vapor diffusion of CH₂Cl₂ with hexanes. Small brown crystals of 9 were isolated in 25% yield. Anal. Calcd for 9·1/2CH₂Cl₂: C, 31.58; H, 4.22; N, 4.27; Fe, 25.53. Found: C, 31.68; H, 4.53; N, 3.86; Fe, 25.51. IR (KBr): 3435 (br), 2980 (w), 2930 (w), 1686 (w), 1663 (w), 1655 (m), 1647 (m), 1637 (m), 1572 (s), 1509 (m), 1491 (m), 1475 (m), 1430 (s), 1344 (m), 1160 (m), 1125 (w), 987 (m), 686 (w), 656 (m), 633 (m), 617 (m), 585 (m), 564 (m), 545 (w), 535 (m), 521 (w), 506 (m), 482 cm⁻¹ (w). Mp 246 °C dec. Electronic spectrum (MeCN) [λ_{max}, nm (ε_M/Fe, cm⁻¹ M⁻¹): 224 (2300), 248 (2503), 288 (2336), 286 (156)].

[Fe₆O₂(C₆H₆NO)₈Cl₄](ClO₄)₂ (10). To a well-stirred solution of FeCl₃·6H₂O (0.32 g, 1.16 mmol) in MeCN (5 mL) was slowly added a solution of 2-pyridylcarbinol (0.38 g, 3.5 mmol) in MeCN (5 mL). Within 2 min, the color of the reaction mixture changed from yellow to orange-yellow. Solid NaClO₄ (0.16 g, 1.16 mmol) was then added and, after 30 min, the crude precipitate was filtered and dried *in vacuo* (0.21 g, 69% yield). Upon concentration of the filtrate, additional product formed as golden brown crystals. The crude product was recrystallized from warm MeCN. Anal. Calcd for [Fe₆O₂(C₆H₆NO)₈Cl₄](ClO₄)₂·MeCN: C, 37.21; H, 3.19; N, 7.81. Found: C, 37.14; H, 3.24; N, 7.81. IR (KBr): 3420 (br), 1610 (s), 1570 (w), 1485 (m), 1455 (w), 1440 (s), 1365 (w), 1285 (m), 1220 (w), 1085 (s), 760 (s), 720 (m), 675 (s), 650 (m), 625 (m), 530 (m), 460 (m), 415 (w) cm⁻¹. Mp 230 °C dec. Electronic spectrum (MeCN) [λ_{max}, nm (ε_M/Fe, cm⁻¹ M⁻¹): 224 (4280), 250 (4846), 296 (sh), 3536].

X-ray Crystallography. Data were collected at low temperature on a Siemens R3m/V automated four-circle diffractometer equipped with a graphite-crystal monochromator. The structures were solved by direct methods (SHELXTL PLUS) and refined by full-matrix least-squares method with scattering factors taken from Cromer and Waber.¹⁹ A summary of the crystallographic data is given in Table I.

[Fe₆O₂(OH)₂(OAc)₁₀(C₇H₁₁N₂O)₂]·4CH₂Cl₂ (9·4CH₂Cl₂). Crystals of 9·4CH₂Cl₂ were grown by vapor diffusion of hexanes into a solution of 9 in CH₂Cl₂ at room temperature. Because of solvent loss, the crystal was covered with a thin layer of epoxy and mounted on a glass fiber. Data were collected at approximately -100 °C employing the 2θ-θ scan method.

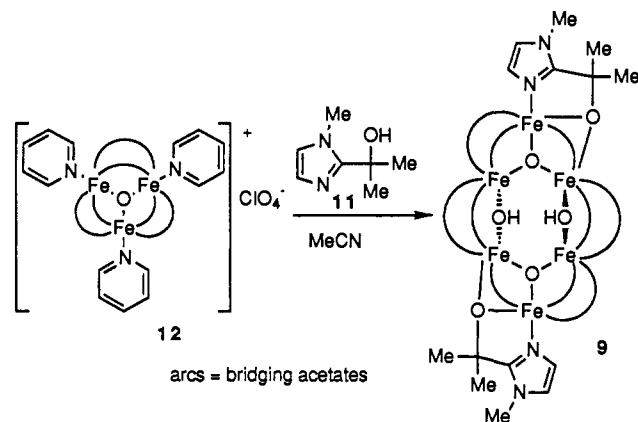
(19) Cromer, D. T.; Waber, J. T. *International Tables for X-ray Crystallography*; Kynoch Press: Birmingham, England, 1974; Vol. IV, Table 2.2A.

The cell parameters were obtained from 23 reflections in the range $15^\circ < 2\theta < 30^\circ$. A systematic search of a full hemisphere of reciprocal space located a set of diffraction maxima with no symmetry or systematic absences indicating a triclinic space group. Subsequent solution and refinement confirmed the centrosymmetric space group $P\bar{1}$. Three standard reflections were monitored after every 100 reflections. The intensity of these reflections decreased by ca. 5% during 32 h of X-ray exposure. An appropriate scale factor was applied to account for the decay. All non-hydrogen atoms were refined anisotropically. Hydrogen atoms were added in ideal positions using the Riding model with U fixed at 0.08 \AA^2 . Four solvent molecules (CH_2Cl_2) were found in the unit cell. A residual peak (1.15 e \AA^{-3}) found near Cl(3) indicated a disordered solvent molecule. No absorption correction was applied. Final positional parameters are available in the supplementary material.

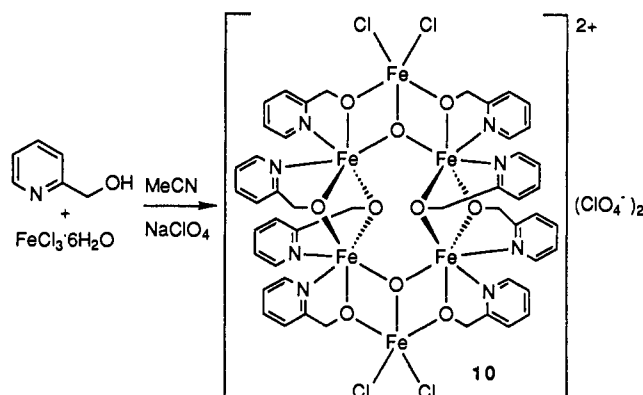
$[\text{Fe}_6\text{O}_2(\text{C}_6\text{H}_6\text{NO})_8\text{Cl}_4](\text{ClO}_4)_2 \cdot 4\text{MeCN}$ (**10-4MeCN**). Crystals of **10-4MeCN** suitable for X-ray diffraction were grown by slow evaporation of the MeCN reaction mixture. The crystal employed for data collection was coated with a thin layer of paratone to prevent solvent loss and mounted on a glass fiber along the longest dimension. Data were collected at 150 K employing the Wyckoff scan method. The cell parameters were obtained from 14 reflections in the range $8^\circ < 2\theta < 15^\circ$. A systematic search of a full hemisphere of reciprocal space located a set of diffraction maxima with no symmetry or systematic absences indicating a triclinic space group. Subsequent solution and refinement confirmed the centrosymmetric space group $P\bar{1}$. Three standard reflections were monitored after every 200 reflections. All of the Fe and Cl atoms were refined anisotropically. All other non-hydrogen atoms were refined isotropically due to large thermal parameters except for O(1), O(2), O(3), O(4), N(5), N(6), C(25), C(26), C(27), and C(28) which were refined anisotropically. Hydrogen atoms were added in ideal positions. Four solvent molecules (MeCN) were found in the unit cell. Final positional parameters are given in the supplementary material.

Results and Discussion

Synthesis. The hexanuclear ferric complex $[\text{Fe}_6\text{O}_2(\text{OH})_2(\text{OAc})_{10}(\text{C}_7\text{H}_{11}\text{N}_2\text{O})_2]$ (**9**) was prepared by the addition of 2-(*N*-methylimidazol-2-yl)-2-hydroxypropane (**11**) to a solution of trinuclear complex **12** in acetonitrile. Concentration *in vacuo* gave a brown oil that was crystallized via vapor diffusion of CH_2Cl_2 with hexanes. It was determined from X-ray crystallography that four CH_2Cl_2 molecules were present in interstitial positions in the crystal. Crystals dried by filtration in air contained less than four CH_2Cl_2 molecules per formula weight. The sample employed in the magnetic susceptibility study analyzed as $9 \cdot \frac{3}{2}\text{CH}_2\text{Cl}_2$.



The hexanuclear complex $[\text{Fe}_6\text{O}_2(\text{C}_6\text{H}_6\text{NO})_8\text{Cl}_4](\text{ClO}_4)_2$ (**10**) was prepared by treatment of an acetonitrile solution of $\text{FeCl}_3 \cdot 6\text{H}_2\text{O}$ with 2-pyridylcarbinol. Addition of NaClO_4 to this solution led to the precipitation of golden-brown complex **10**. From X-ray crystallography it was determined that four acetonitrile molecules were present per formula weight in the crystal. However, some of these solvent molecules were lost upon drying of the crystals in air. The sample used in the magnetic susceptibility measurements analyzed to have the composition of **10-4MeCN**.



Crystal Structure of $[\text{Fe}_6\text{O}_2(\text{OH})_2(\text{OAc})_{10}(\text{C}_7\text{H}_{11}\text{N}_2\text{O})_2] \cdot 4\text{CH}_2\text{Cl}_2$ (9-4CH}_2\text{Cl}_2).** The structure of **9** is shown in Figure 1. Its structure is analogous to previously reported complex **5**.⁸ It contains a planar array of six Fe^{III} ions with the maximum deviation from planarity of an iron ion being $0.03(1) \text{ \AA}$. The complex can be viewed as two trinuclear μ_3 -oxo-bridged subunits bridged by two μ_2 -hydroxo and four μ_2 -acetato ligands. The bridging hydroxo group, O(11), is $0.805(4) \text{ \AA}$ above the central Fe_4 plane [Fe(2), Fe(2A), Fe(3), Fe(3A)] while the bridging hydroxo oxygen makes a $123.9(2)^\circ$ angle with the two iron atoms Fe(2) and Fe(3A). In each triangular subunit the triply bridging oxide lies $0.184(4) \text{ \AA}$ below the plane defined by the three iron atoms [Fe(1), Fe(2), Fe(3)].**

The trinuclear iron subunits of **9** are asymmetrical due to their differing coordination environments. The three iron atoms form a scalene triangle with sides of the following lengths: [Fe(1)–Fe(2)], $3.238(2) \text{ \AA}$; [Fe(2)–Fe(3)], $3.579(2) \text{ \AA}$; and [Fe(1)–Fe(3)], $2.947(2) \text{ \AA}$. The triply bridging oxide ion is $1.902(3) \text{ \AA}$ from Fe(1), $1.872(3) \text{ \AA}$ from Fe(2), and $1.949(4) \text{ \AA}$ from Fe(3). The coordination around Fe(1) is distorted from octahedral geometry due to the small bite angle of the hydroxyimidazole ligand [N(1)–Fe(1)–O(1), $77.6(2)^\circ$]. The μ_2 -alkoxo oxygen atom also causes a less severe distortion from octahedral geometry at Fe(3) [O(1)–Fe(3)–O(2), $80.6(1)^\circ$]. The angles around Fe(2) are closer to octahedral geometry [$85.2(1)^\circ$ – $97.1(1)^\circ$]. The metal ligand bond distances of **9** are typical for high-spin Fe^{III} complexes. Selected bond lengths and angles are presented in Table II.

Crystal Structure of $[\text{Fe}_6\text{O}_2(\text{C}_6\text{H}_6\text{NO})_8\text{Cl}_4](\text{ClO}_4)_2 \cdot 4\text{MeCN}$ (10-4MeCN**).** The structure of the cation of complex **10** is shown in Figure 2. Complex **10** crystallizes in the $P\bar{1}$ space group and possesses a crystallographic center of inversion, thus making only three of the six iron centers unique. The six iron ions are arranged in a chair conformation with the four central iron atoms [Fe(1), Fe(2), Fe(1A), Fe(2A)] forming a plane. The two terminal iron atoms [Fe(3) and Fe(3A)] are $1.579(1) \text{ \AA}$ above and below the central iron plane, respectively. Fe(1) and Fe(2A) are bridged by two alkoxo groups. The alkoxo oxygen atoms, O(8A) and O(9), are positioned above [$1.195(2) \text{ \AA}$] and below [$1.200(2) \text{ \AA}$] the central Fe_4 plane. The Fe–O–Fe angles are $105.4(2)^\circ$ and $105.2(2)^\circ$ while the O–Fe–O angles are $74.1(1)^\circ$ and $73.7(1)^\circ$, thus creating a rhombus arrangement in the Fe_2O_2 unit.

As in complex **9**, the six iron ions in complex **10** may be viewed as two asymmetric triangular Fe_3 – μ_3 -oxo subunits bridged together by alkoxo groups. The three iron centers form an isosceles triangle with sides of length $3.054(1) \text{ \AA}$ [Fe(1)–Fe(3)], $3.040(1) \text{ \AA}$ [Fe(2)–Fe(3)], and $3.688(1) \text{ \AA}$ [Fe(1)–Fe(2)]. The μ_3 -oxo atom, O(5), is bound to Fe(3) with a bond distance of $1.947(4) \text{ \AA}$ while the bond distances to Fe(1) and Fe(2) are shorter [$1.905(3) \text{ \AA}$ and $1.907(3) \text{ \AA}$, respectively]. The Fe(2)–O(5)–Fe(3) and Fe(1)–O(5)–Fe(3) angles are $104.9(1)^\circ$ and $104.1(2)^\circ$, while the Fe(1)–O(5)–Fe(2) angle is much larger with a value of $150.7(2)^\circ$.

The two terminal iron ions are five coordinate, possessing a slightly distorted trigonal-bipyramidal geometry. The six-

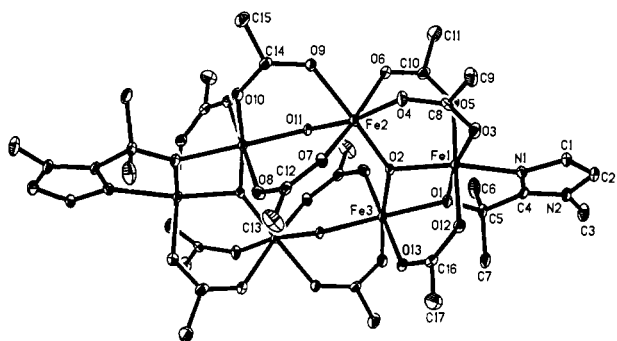


Figure 1. ORTEP drawing of the Fe^{III}_6 complex $[\text{Fe}_6\text{O}_2(\text{OH})_2(\text{OAc})_{10}(\text{C}_7\text{H}_{11}\text{N}_2\text{O})_2] \cdot 4\text{CH}_2\text{Cl}_2$ ($9 \cdot 4\text{CH}_2\text{Cl}_2$). Solvent molecules have been omitted for clarity.

Table II. Selected Bond Distances (Å) and Angles (deg) for the Complex $[\text{Fe}_6\text{O}_2(\text{OH})_2(\text{OAc})_{10}(\text{C}_7\text{H}_{11}\text{N}_2\text{O})_2] \cdot 4\text{CH}_2\text{Cl}_2$ ($9 \cdot 4\text{CH}_2\text{Cl}_2$)

Bonds			
Fe(1)–O(1)	2.004(4)	Fe(2)–O(11)	1.978(3)
Fe(1)–O(2)	1.902(3)	Fe(3)–O(1)	2.011(3)
Fe(1)–O(3)	1.990(4)	Fe(3)–O(2)	1.949(4)
Fe(1)–O(5)	2.052(4)	Fe(3)–O(13)	2.059(4)
Fe(1)–O(12)	2.084(4)	Fe(3)–O(8A)	2.057(4)
Fe(1)–N(1)	2.075(4)	Fe(3)–O(10A)	2.015(4)
Fe(2)–O(2)	1.872(3)	Fe(3)–O(11A)	1.964(3)
Fe(2)–O(4)	2.062(4)	Fe(1)···Fe(3)	2.947(2)
Fe(2)–O(6)	2.037(4)	Fe(1)···Fe(2)	3.238(2)
Fe(2)–O(7)	2.031(4)	Fe(2)–Fe(3)	3.579(2)
Fe(2)–O(9)	2.094(4)	Fe(3)···Fe(2A)	3.479(2)
Angles			
O(1)–Fe(1)–O(2)	81.9(1)	O(6)–Fe(2)–O(7)	167.9(2)
O(1)–Fe(1)–O(3)	170.5(1)	O(6)–Fe(2)–O(9)	85.7(1)
O(1)–Fe(1)–O(5)	96.6(2)	O(6)–Fe(2)–O(11)	91.7(1)
O(1)–Fe(1)–O(12)	90.2(2)	O(4)–Fe(2)–O(6)	85.2(1)
O(1)–Fe(1)–N(1)	77.6(2)	O(4)–Fe(2)–O(7)	86.2(1)
O(3)–Fe(1)–O(5)	87.7(2)	O(4)–Fe(2)–O(9)	85.5(1)
O(3)–Fe(1)–O(12)	85.4(2)	O(4)–Fe(2)–O(11)	170.6(1)
O(3)–Fe(1)–N(1)	194.2(2)	O(7)–Fe(2)–O(9)	85.2(1)
O(2)–Fe(1)–O(3)	106.4(1)	O(7)–Fe(2)–O(11)	96.5(1)
O(2)–Fe(1)–O(5)	92.8(1)	O(9)–Fe(2)–O(11)	85.7(1)
O(2)–Fe(1)–O(12)	89.2(1)	O(1)–Fe(3)–O(2)	80.6(1)
O(2)–Fe(1)–N(1)	159.5(2)	O(1)–Fe(3)–O(13)	89.1(1)
O(5)–Fe(1)–O(12)	173.1(2)	O(1)–Fe(3)–O(8A)	91.1(1)
O(5)–Fe(1)–N(1)	89.2(2)	O(1)–Fe(3)–O(10A)	134.6(1)
O(12)–Fe(1)–N(1)	91.3(2)	O(1)–Fe(3)–O(11A)	176.4(2)
O(2)–Fe(2)–O(4)	97.1(1)	O(13)–Fe(3)–O(8A)	91.1(1)
O(2)–Fe(2)–O(6)	94.9(1)	O(13)–Fe(3)–O(10A)	91.9(2)
O(2)–Fe(2)–O(7)	94.6(2)	O(13)–Fe(3)–O(11A)	87.9(1)
O(2)–Fe(2)–O(9)	177.4(1)	O(2)–Fe(3)–O(13)	88.8(2)
O(2)–Fe(2)–O(11)	91.7(1)	O(2)–Fe(3)–O(8A)	90.3(2)
O(2)–Fe(3)–O(10A)	173.7(1)	Fe(2)–O(11)–Fe(3A)	123.9(2)
O(2)–Fe(3)–O(11A)	97.5(1)	Fe(1)–O(1)–Fe(3)	94.5(2)
O(8A)–Fe(3)–O(10A)	89.0(2)	Fe(1)–O(2)–Fe(2)	118.2(2)
O(8A)–Fe(3)–O(11A)	91.9(1)	Fe(2)–O(2)–Fe(3)	139.0(1)
O(10A)–Fe(3)–O(11A)	88.8(1)	Fe(1)–O(2)–Fe(3)	99.8(1)

coordinate iron ions which make up the central plane are very distorted from an octahedral geometry. The angles range from $73.7(1)^\circ$ to $111.3(1)^\circ$ for the cis and $150.3(2)^\circ$ to $172.8(1)^\circ$ for the trans ligands. This deviation, far from the expected values of 90.0° and 180.0° , is due to the steric constraints of the coordinated alkoxy-pyridine ligands. The metal–ligand bond distances are typical for high-spin $\text{Fe}(\text{III})$ complexes. Selected bond lengths and angles are presented in Table III.

Comparison of Structures of Hexanuclear Ferric Complexes.

The ten hexanuclear ferric complexes can be grouped into six different structural classes (see Figure 3). Complexes 1, 5, and 9 all possess a planar framework of the six iron ions (see A in Figure 3). The six iron centers of Lippard's two complexes, 2 and 3, are in a twisted boat-like configuration (see B in Figure 3). A third configuration, with the six iron centers in a chair, is illustrated by complex 10 (see C in Figure 3). Complexes of

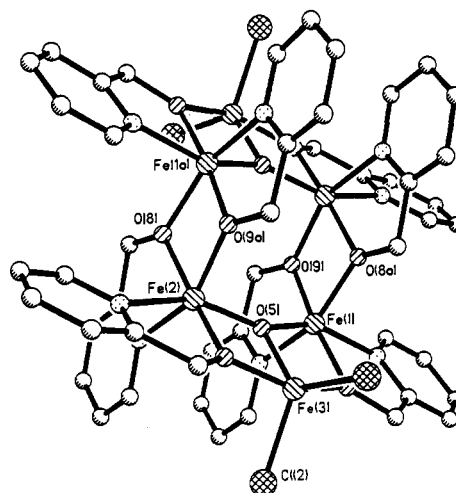


Figure 2. ORTEP drawing of the Fe^{III}_6 cationic complex in $[\text{Fe}_6\text{O}_2(\text{C}_6\text{H}_6\text{NO})_8\text{Cl}_4](\text{ClO}_4)_2 \cdot 4\text{MeCN}$ ($10 \cdot 4\text{MeCN}$). Solvent molecules and ClO_4^- counteranions are omitted for clarity.

Table III. Selected Bond Distances (Å) and Angles (deg) for the Complex $[\text{Fe}_6\text{O}_2(\text{C}_6\text{H}_6\text{NO})_8\text{Cl}_4](\text{ClO}_4)_2 \cdot 4\text{MeCN}$

Bonds			
Fe(1)–O(5)	1.907(3)	Fe(2)–O(8)	1.992(4)
Fe(1)–O(9)	1.984(4)	Fe(2)–O(9A)	1.999(3)
Fe(1)–O(6)	1.978(4)	Fe(2)–N(2)	2.155(4)
Fe(1)–O(8A)	1.988(3)	Fe(2)–N(3)	2.154(4)
Fe(1)–N(1)	2.157(4)	Fe(3)–Cl(2)	2.227(2)
Fe(1)–N(4)	2.142(4)	Fe(3)–Cl(3)	2.243(2)
Fe(3)–O(5)	1.947(4)	Fe(1)···Fe(2)	3.688(2)
Fe(3)–O(7)	1.973(3)	Fe(1)···Fe(3)	3.040(2)
Fe(3)–O(6)	1.985(3)	Fe(2)···Fe(3)	3.054(2)
Fe(2)–O(5)	1.905(3)	Fe(1)···Fe(2A)	3.165(2)
Fe(2)–O(7)	1.977(4)		
Angles			
O(5)–Fe(1)–O(6)	78.3(1)	O(7)–Fe(2)–O(9A)	98.1(1)
O(6)–Fe(1)–O(9)	172.8(1)	N(2)–Fe(2)–O(9A)	92.6(1)
O(6)–Fe(1)–N(1)	75.8(1)	O(5)–Fe(2)–O(7)	77.3(1)
O(5)–Fe(1)–N(4)	93.8(1)	O(7)–Fe(2)–O(8)	169.7(1)
O(9)–Fe(1)–N(4)	76.7(1)	O(7)–Fe(2)–N(2)	75.9(2)
O(5)–Fe(1)–O(8A)	99.0(1)	O(5)–Fe(2)–N(3)	91.8(1)
O(9)–Fe(1)–O(8A)	74.1(1)	O(8)–Fe(2)–N(3)	76.6(1)
N(4)–Fe(1)–O(8A)	150.6(2)	O(5)–Fe(2)–O(9A)	99.2(1)
O(5)–Fe(1)–O(9)	108.8(1)	O(8)–Fe(2)–O(9A)	73.7(1)
O(5)–Fe(1)–N(1)	153.1(1)	N(3)–Fe(2)–O(9A)	150.3(2)
O(9)–Fe(1)–N(1)	97.3(1)	Cl(2)–Fe(3)–Cl(3)	112.9(1)
O(6)–Fe(1)–N(4)	104.6(1)	Cl(3)–Fe(3)–O(5)	126.1(1)
N(1)–Fe(1)–N(4)	85.8(1)	Cl(3)–Fe(3)–O(6)	95.8(1)
O(6)–Fe(1)–O(8A)	103.8(1)	Cl(2)–Fe(3)–O(7)	98.5(1)
N(1)–Fe(1)–O(8A)	94.1(1)	O(5)–Fe(3)–O(7)	76.4(1)
O(5)–Fe(2)–O(8)	109.7(1)	Cl(2)–Fe(3)–O(5)	121.0(1)
O(5)–Fe(2)–N(2)	151.9(2)	Cl(2)–Fe(3)–O(6)	97.6(1)
O(8)–Fe(2)–N(2)	98.0(1)	O(5)–Fe(3)–O(6)	77.2(1)
O(7)–Fe(2)–N(3)	111.3(1)	Cl(3)–Fe(3)–O(7)	97.2(1)
N(2)–Fe(2)–N(3)	90.3(1)	O(6)–Fe(3)–O(7)	153.4(2)
Fe(1)–O(5)–Fe(2)	150.7(2)	Fe(1)–O(9)–Fe(2A)	105.2(2)
Fe(1)–O(5)–Fe(3)	104.1(2)	Fe(2)–O(9)–Fe(1A)	105.4(2)
Fe(2)–O(5)–Fe(3)	104.9(1)		

the type A, B, and C may all be viewed as two $[\text{Fe}_3-\mu_3\text{-O}]$ moieties with multiple hydroxo or alkoxo bridges between the bases of the triangular subunits. Complex 8, which also contains two $[\text{Fe}_3-\mu_3\text{-O}]$ subunits, possesses a slightly different orientation of the triangular subunits than found in A, B, and C (see D in Figure 3). The triangular subunits in this complex are positioned in parallel planes. The apical iron center of one triangle is bridged by two μ_3 -hydroxo groups to the two base iron centers of the parallel triangle. In contrast to the triangular arrangement, complexes 4 and 6 have the six iron ions arranged octahedrally around a μ_6 -oxo center (see E in Figure 3) while complex 7 can be viewed as the fusion of two $[\text{Fe}_4-\mu_4\text{-O}]$ units (see F in Figure 3).

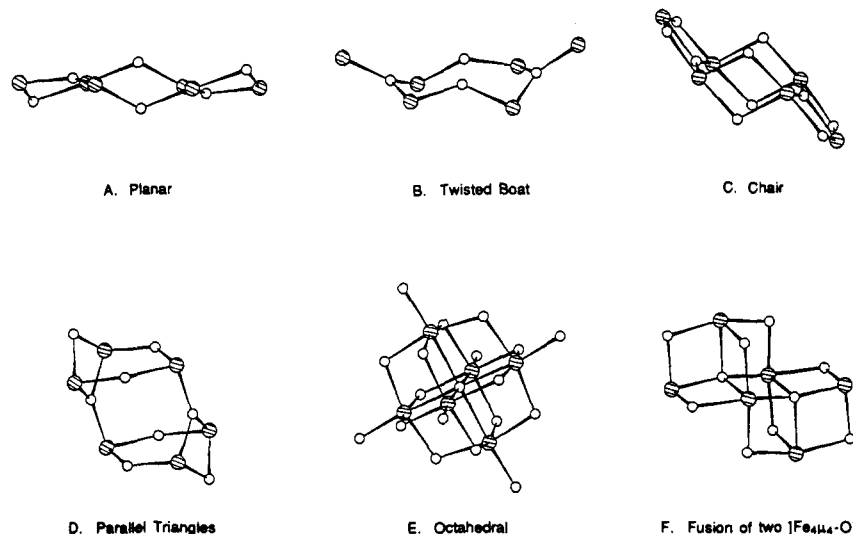


Figure 3. The iron-oxo cores of the six different structural classes observed for hexanuclear ferric complexes. Iron atoms are cross hatched.

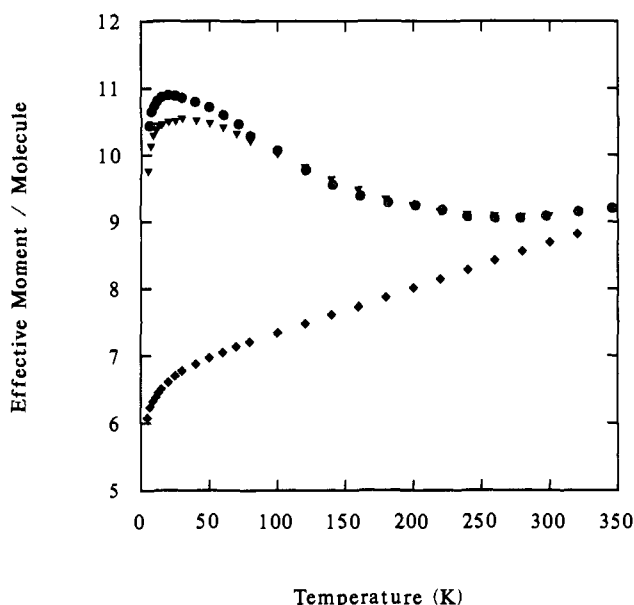


Figure 4. Plot of effective magnetic moment per Fe^{III}_6 complex versus temperature for three complexes: (▼) $[\text{Fe}_6\text{O}_2(\text{OH})_2(\text{OAc})_{10}(\text{C}_7\text{H}_{11}\text{N}_2\text{O}_2)] \cdot 3/2\text{CH}_2\text{Cl}_2$ ($9^{3/2}\text{CH}_2\text{Cl}_2$); (○) $[\text{Fe}_6\text{O}_2(\text{OH})_2(\text{OAc})_{10}(\text{C}_{10}\text{H}_{13}\text{N}_4\text{O}_2)] \cdot \text{CH}_2\text{Cl}_2$ ($5 \cdot \text{CH}_2\text{Cl}_2$); and (◆) $[\text{Fe}_6\text{O}_2(\text{C}_6\text{H}_6\text{NO})_8\text{Cl}_4](\text{ClO}_4)_2 \cdot \text{MeCN}$ ($10 \cdot \text{MeCN}$).

Variable-Temperature Magnetic Susceptibility. A polycrystalline sample of complex $9^{3/2}\text{CH}_2\text{Cl}_2$ was embedded in parafilm to eliminate torquing in a magnetic field and the DC susceptibility was measured in a field of 10.0 kG in the 5.00–300.0 K range. Figure 4 shows a plot of the effective magnetic moment (μ_{eff}) per molecule versus temperature. At 300.0 K μ_{eff} /molecule is $9.10 \mu_{\text{B}}$ and as the temperature is decreased μ_{eff} /molecule increases to a maximum of $10.55 \mu_{\text{B}}$ at 30.0 K. A further decrease in the temperature leads to a decrease in μ_{eff} /molecule to $9.77 \mu_{\text{B}}$ at 5.00 K. As can be seen in Figure 4, the plot of μ_{eff} /molecule versus temperature for complex 9 looks very similar to that reported⁸ for complex 5 . This is reasonable in view of the fact that the two complexes are isostructural. The appearance of the μ_{eff} /molecule versus temperature plots for complexes 5 and 9 probably reflects the situation where at low temperatures only the $S = 5$ ground state is populated. The spin-only μ_{eff} value for a $S = 5$ state is $10.95 \mu_{\text{B}}$. The drop in μ_{eff} /molecule which is seen below 30.0 K for complex 9 would then be due to a combination of zero-field and Zeeman splitting of the $S = 5$ ground state.

A plot of μ_{eff} /molecule versus temperature (5.01–320.0 K) is shown in Figure 4 for a polycrystalline sample of complex $10 \cdot \text{MeCN}$ embedded in parafilm and in an external field of 10.0 kG. At 320.0 K μ_{eff} /molecule is $8.82 \mu_{\text{B}}$ and with decreasing temperature μ_{eff} /molecule decreases to $6.08 \mu_{\text{B}}$ at 5.01 K. The ground state of complex 10 must have a smaller value of S_{T} than those for complexes 5 and 9 .

No magnetic susceptibility data have been reported for hexanuclear iron complexes 1 , 3 , 4 , and 6 . Complex 2 , $[\text{Fe}_6(\mu_3\text{-O})_2(\mu_2\text{-OH})_2(\mu_2\text{-O}_2\text{CPh})_{12}(\text{OH})_2(1,4\text{-dioxane})]$, was reported¹⁹ to have a μ_{eff} /molecule of $7.33 \mu_{\text{B}}$ at 300 K, which gradually decreases to $0.62 \mu_{\text{B}}$ at 2.0 K. Micklitz and Lippard¹⁰ concluded that complex 2 has a $S_{\text{T}} = 0$ ground state. Complex 8 was reported by Harding et al.¹⁵ to exhibit an increase in $\mu_{\text{eff}}/\text{Fe}$ with decreasing temperature from a value of $4.02 \mu_{\text{B}}$ at 300 K to $\sim 4.4 \mu_{\text{B}}$ at ~ 70 K. A slight decrease is then observed until ~ 20 K where μ_{eff} increases sharply to give a maximum value of $4.81 \mu_{\text{B}}$ at 5 K. Nair and Hagen¹⁴ provided detailed variable-temperature and variable-field susceptibility data for complex $7 \cdot (\text{CF}_3\text{SO}_3)_2 \cdot 2\text{MeOH}$. In an applied field of 2 kG the μ_{eff} /molecule for this salt of complex 7 was found to be $8.61 \mu_{\text{B}}$ at 299.6 K. Upon decreasing the temperature the μ_{eff} /molecule increases to $\sim 11.4 \mu_{\text{B}}$ at ~ 10 K. At the lowest temperature and 55 kG the reduced magnetization ($M/N\mu_{\text{B}}$, where M is the magnetization, N is Avogadro's number, and μ_{B} is the Bohr magneton) approached saturation at a value of almost $11 \mu_{\text{B}}$. The maximum saturation magnetization that a $S_{\text{T}} = 5$ ground state complex should give is $10 \mu_{\text{B}}$.

Variable-Field Magnetization Studies. Measurements of magnetization were carried out for complexes 9 and 10 at various magnetic fields in order to characterize the ground state of these two complexes. The magnetization of a parafilm-embedded polycrystalline sample of complex $9^{3/2}\text{CH}_2\text{Cl}_2$ was measured at 50.0 and 10.0 kG in the range of 2.00–30.0 K and at fields of 40.0, 30.0, 20.0, and 5.00 kG in the range of 2.00–4.00 K. These data are illustrated in Figure 5 as a plot of reduced magnetization versus H/T . At 50.0 kG and 2.00 K the value of $M/N\mu_{\text{B}}$ saturates at a value of $9.63 \mu_{\text{B}}$. The nonsuperimposability of the six isofield data sets indicates that the ground state has appreciable zero-field splitting.

The magnetization for a hexanuclear ferric complex may be calculated by using the basic thermodynamic relation²⁰ given in eq 1. The energies of the various spin sublevels are obtained by diagonalization of the spin Hamiltonian matrix, including Zeeman interactions and axial zero-field splitting. Thus, in fitting the data it is assumed that there is only one state with total spin S

(20) Vermaas, A.; Groenveld, W. L. *Chem. Phys. Lett.* **1984**, *27*, 583.

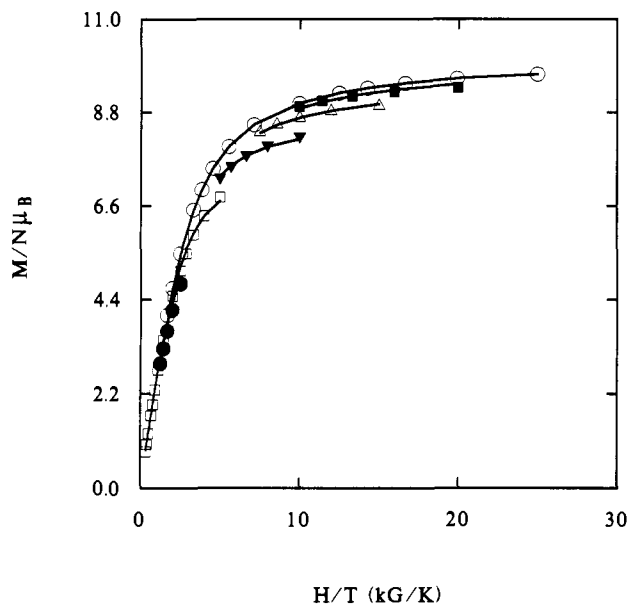


Figure 5. Plots of reduced magnetization ($M/N\mu_B$) versus magnetic field in units of temperature (H/T) for $[\text{Fe}_6\text{O}_2(\text{OH})_2(\text{OAc})_{10}(\text{C}_7\text{H}_{11}\text{N}_2\text{O})_2] \cdot 3/2\text{CH}_2\text{Cl}_2$ ($9^{3/2}\text{CH}_2\text{Cl}_2$): (○) 50.0 kG; (□) 40.0 kG; (△) 30.0 kG; (▽) 20.0 kG; (■) 10.0 kG; (●) 5.00 kG. The solid lines represent a least-squares fit of the data with a full-matrix diagonalization technique.

thermally occupied and the spin Hamiltonian matrix is of dimensions $(2S + 1) \times (2S + 1)$.

$$M = N \sum_{i=1}^P \left(\frac{-\delta E_i}{\delta H} \right) \exp(-E_i/kT) / \sum_{i=1}^P \exp(-E_i/kT) \quad (1)$$

The data shown in Figure 5 for complex $9^{3/2}\text{CH}_2\text{Cl}_2$ were least-squares fit to eq 1. The spin of the ground state was taken to be $S = 5$. The solid lines in Figure 5 represent the best least-squares fit of the data, which gave parameters of $g = 2.0$ and $D = 0.32 \text{ cm}^{-1}$. The parameter D characterizes the axial ($D\hat{S}_z^2$) zero-field splitting in the $S = 5$ ground state. It can be concluded that complex $9^{3/2}\text{CH}_2\text{Cl}_2$ has a $S = 5$ ground state which is relatively isolated from excited spin states.

In Figures 6 and 7 are given plots of reduced magnetization versus H/T for a parafilm-embedded polycrystalline sample of complex 10-MeCN . Three isofield data sets measured at 20.0, 30.0, and 50.0 kG are shown in Figure 6. At 50.0 kG and the lowest temperature $M/N\mu_B$ tends to saturate at a value of $\sim 5.6 \mu_B$. These three data sets were least-squares fit to eq 1. The g value was fixed at 2.0. Fitting the 20.0, 30.0, and 50.0-kG data assuming a $S = 3$ ground state gave $D = -0.72 \text{ cm}^{-1}$ for the axial zero-field splitting parameter. As can be seen in Figure 6, this fit is not very good in comparison to the fit of the more extensive data set shown in Figure 5 for complex $9^{3/2}\text{CH}_2\text{Cl}_2$.

The data shown in Figure 7 for complex 10-MeCN were measured at fields of 0.50, 1.00, 2.00, 3.00, 5.00, and 10.0 kG. Least-squares fitting of these data, assuming that $S = 3$ for the only state populated and with $g = 2.0$ fixed, gave for the only remaining parameter $D = +3.1 \text{ cm}^{-1}$. The solid lines in Figure 7 show that this fit is reasonable. The appreciable variation in the fitting parameter D with fitting their high- or low-field magnetization data and the quite large values of D obtained for the low-field data are indications that complex 10-MeCN does not have only one state populated in these temperature and magnetic field ranges.

Theoretical Calculations of Spin-State Orderings. In an effort to understand the differences between the two $S = 5$ ground state complexes **5** and **9** and complex **10** which has a ground state with approximately $S = 3$ in an appreciable magnetic field, theoretical

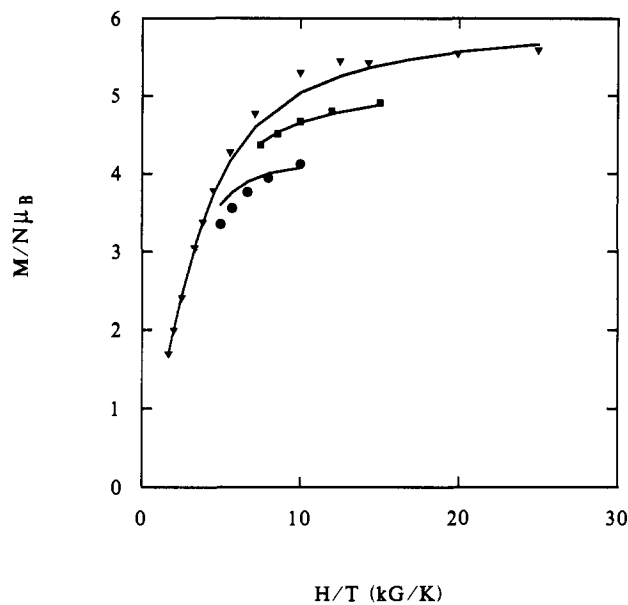


Figure 6. Plots of reduced magnetization ($M/N\mu_B$) versus magnetic field in units of temperature (H/T) for $[\text{Fe}_6\text{O}_2(\text{C}_6\text{H}_6\text{NO})_8\text{Cl}_4](\text{ClO}_4)_2 \cdot \text{MeCN}$ (10-MeCN): (▽) 50.0 kG; (■) 30.0 kG; and (●) 20.0 kG. The solid lines represent a least-squares fit of the data with a full-matrix diagonalization technique.

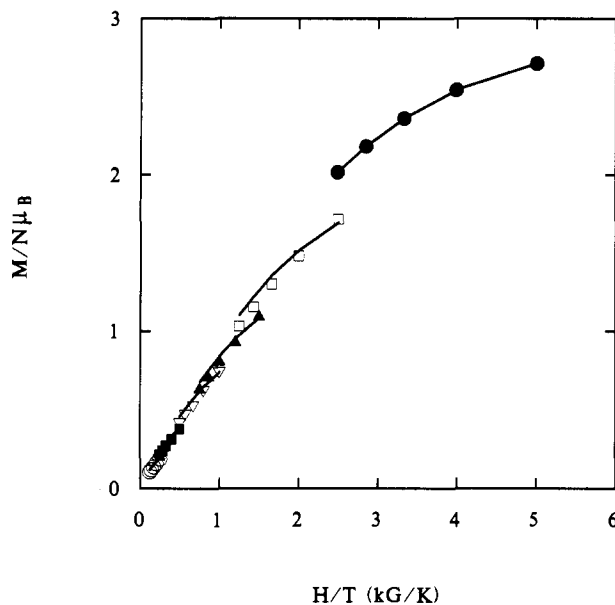


Figure 7. Plots of reduced magnetization ($M/N\mu_B$) versus magnetic field in units of temperature (H/T) for $[\text{Fe}_6\text{O}_2(\text{C}_6\text{H}_6\text{NO})_8\text{Cl}_4](\text{ClO}_4)_2 \cdot \text{MeCN}$ (10-MeCN): (○) 10.0 kG; (□) 5.00 kG; (△) 3.00 kG; (▽) 2.00 kG; (■) 1.00 kG; and (●) 0.50 kG. The solid lines represent a least-squares fit of the data with a full-matrix diagonalization technique.

calculations were carried out. At the outset it has to be appreciated that such a calculation on a Fe^{III}_6 complex is an enormous undertaking.²¹ Such a complex has 4332 different spin states with a total spin ranging from $S = 0$ to 15. In Table IV is given the distribution of the 4332 different spin states. For example, there is only 1 state with $S = 15$, 5 states with $S = 14$, and 111 states with $S = 0$. The most prevalent is $S = 4$ with 609 states.

Theoretical calculations of the spin-state orderings in a Fe^{III}_6 complex were carried out by means of the technique described by two of the authors.²² The total spin Hamiltonian matrix (46656×46656) was taken as blocked-diagonalized where the largest

(21) Delfo, C. D.; Gatteschi, D.; Pardi, L. *Comments Inorg. Chem.*, 1993, in press.

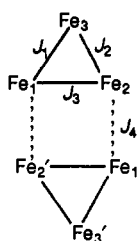
(22) Gatteschi, D.; Pardi, L. *Gazz. Chim. Ital.* 1993, 123, 231.

Table IV. The Distribution of Spin States for a Fe^{III}_6 Complex^a

total spin, S_T	no. of states	total spin, S_T	no. of states
15	1	7	405
14	5	6	505
13	15	5	581
12	35	4	609
11	70	3	575
10	126	2	475
9	204	1	315
8	300	0	111

^a There are 4332 different spin states.

block is 609×609 for the $S = 4$ states. Irreducible tensor operator techniques²³ were used to evaluate the matrix elements (coupled basis set) in the various blocks where S varies from 0 to 15. Since the Fe^{III}_6 complexes are centrosymmetric there are four different types of pairwise magnetic exchange interactions in the complex as delineated in the following diagram: In each μ_3 -oxo-bridged



Fe^{III}_3 triangle there are three different pairwise exchange interactions parametrized with J_1 , J_2 , and J_3 . The two $\text{Fe}^{\text{III}}_3\text{O}$ triangles interact via hydroxo or alkoxo bridges in the J_4 -type interactions. Since all of these four interactions (J_1 , J_2 , J_3 , and J_4) involve pairwise interactions between two high-spin Fe^{III} ions, they are all expected to be antiferromagnetic exchange interactions.

The 10.0-kG variable-temperature susceptibility data (Figure 4) for complex **5** which has an $S_T = 5$ ground state and complex **10** which has a ground state of considerably smaller total spin were analyzed in the theoretical calculations. In both cases only the data in the 20–320 K range were analyzed, for the data at lower temperatures are affected by Zeeman and zero-field interactions. The least-squares fitting procedure was carried out by coupling the computer program CLUMAG, recently developed by two of the authors²² to calculate the matrix elements by irreducible tensor operators techniques, to the minimization MINUIT library.

At first, least-squares fits were attempted for both data sets by assuming all three exchange interactions in each Fe_3O triangle are equal, *i.e.*, $J_1 = J_2 = J_3 \equiv J$. In this case, there are two parameters J and J_4 . Only very poor fits of the two data sets could be obtained with this assumption of equilateral Fe_3O triangles. At the next level it was assumed that, relative to the exchange interactions present in complexes **5** and **10**, each Fe_3O triangle was an isosceles triangle. Two different cases of isosceles triangles must be distinguished, one in which $J_1 = J_2 \neq J_3$ and the other in which $J_1 \neq J_2 = J_3$. These two exchange topologies give rise to completely different magnetochemical behaviors. In the first case, calculations have shown that an $S_T = 0$ spin state is the ground state for a Fe^{III}_6 complex independent of the three different exchange parameters J_1 ($=J_2$), J_3 , and J_4 . On the other hand, calculations show that when $J_1 \neq J_2 = J_3$, the spin states with S values ranging from $S_T = 5$ to 0 can be stabilized as the ground state of a Fe^{III} complex, depending on the value of the J_1/J_2 ratio.

Complex **5** is isostructural to complex **9**. With reference to the above diagram, the iron ions Fe_1 and Fe_2 are involved in exchange interactions which are dominantly propagated by one

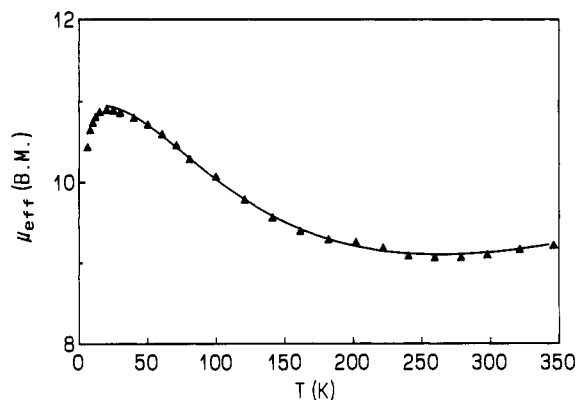


Figure 8. Plot of effective magnetic moment per Fe^{III}_6 complex versus temperature for a polycrystalline sample of $[\text{Fe}_6\text{O}_2(\text{OH})_2(\text{OAc})_{10}(\text{C}_{10}\text{H}_{13}\text{N}_4\text{O})_2] \cdot \text{CH}_2\text{Cl}_2$ (**5**· CH_2Cl_2) in an external field of 10.0 kG. The data are from ref 15. The solid line results from a theoretical fit. See the text for details.

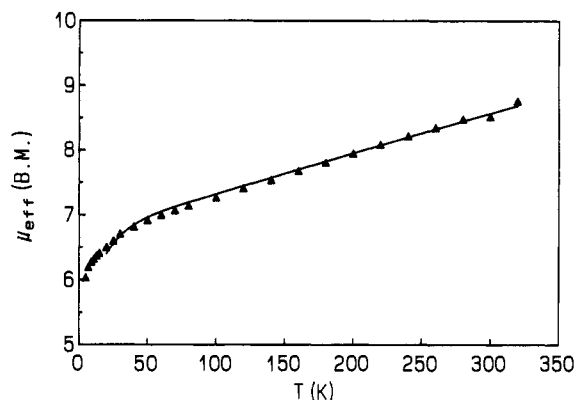


Figure 9. Plot of effective magnetic moment per Fe^{III}_6 complex versus temperature for a polycrystalline sample of $[\text{Fe}_6\text{O}_2(\text{C}_6\text{H}_6\text{NO})_8\text{Cl}_4] \cdot (\text{ClO}_4)_2 \cdot \text{MeCN}$ (**10**· MeCN) in an external field of 10.0 kG. The solid lines result from a theoretical fit. See the text for details.

μ_3 -oxide ion. The Fe_2 and Fe_3 ions are also bridged by one μ_3 -oxide ion, whereas the Fe_1 and Fe_3 ions are bridged by one μ_3 -oxide ion and one μ_2 -alkoxide ion as far as the exchange interactions are concerned. As a consequence the coupling scheme where $J_1 \neq J_2 = J_3$ was employed to fit the data for complex **5**. In Figure 8 is shown the best fit obtained for the 10.0-kG data of complex **5**. The g value was held fixed at 2.0. As can be seen, the fit accommodates very well all of the data in the 20–320 K range. For complex **5** the best fitting parameters were found to be $J_1 = -5.6(5) \text{ cm}^{-1}$, $J_2 = J_3 = -38(1) \text{ cm}^{-1}$, and $J_4 = -7.5(1) \text{ cm}^{-1}$. According to these fitting parameters complex **5** has a $S_T = 5$ ground state well separated in energy from the first excited state, an $S_T = 4$ state at 69.9 cm^{-1} . A plot of the energies of all the 4332 different spin states for complex **5** is available in the Supplementary Material.

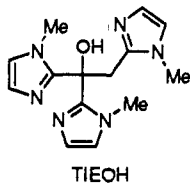
The 20–320 K data for complex **10** were fit trying several different coupling schemes. The best fit of the data is illustrated in Figure 9. The solid line in this figure fits well the data and corresponds to the fitting parameters of $J_1 = J_2 = -18(1) \text{ cm}^{-1}$, $J_3 = -52(2) \text{ cm}^{-1}$, and $J_4 = -3(2) \text{ cm}^{-1}$. The g value was held fixed at 2.0. From the above fitting parameters it can be calculated that complex **10** has an $S_T = 0$ ground state with the following low-energy excited states: $S_T = 1$ at 1.6 cm^{-1} , $S_T = 2$ at 4.5 cm^{-1} , $S_T = 3$ at 7.5 cm^{-1} , and $S_T = 4$ at 10.0 cm^{-1} . In Figure 10 is shown a plot of the distribution of states which are found within 100 cm^{-1} of the $S_T = 0$ ground state as calculated with the above fitting parameters.

Several comments can be made about these theoretical fitting results. First, for complex **10** it is pleasing to find that the

(23) Silver, B. L. *Irreducible Tensor Methods*; Academic Press: New York, 1976.

theoretical analysis shows there are several low-energy excited spin states as suggested by the variable-field magnetization results. However, the fitting parameters give an $S_T = 0$ ground state with $S_T = 2$ and $S_T = 3$ states at energies of 4.5 and 7.5 cm^{-1} , respectively. These results are only qualitatively in agreement with the experimental magnetization data, which indicate that in even small fields such as 500 G the magnetization data run in the 2–4 K range reflect a spin in the range of $S_T = 3$. Obviously, zero-field interactions are very important. The theoretical calculations do not incorporate zero-field interactions. The second point to make about the above theoretical analysis is that it was necessary to make an assumption about the topology of the coupling scheme in order to make the problem tractable. Thus, the X-ray structural results⁸ for complex **5** indicate that each Fe_3O triangle is a scalene triangle. Even though the Fe_3O triangles of complex **10** are closer to isosceles, it could well be that $J_1 \neq J_2 \neq J_3$ for both of these complexes. However, it is not feasible to employ four different exchange interaction parameters to fit the data for these complexes.

In spite of these difficulties and assumptions it must be noted that the exchange parameters evaluated as fitting parameters for complexes **5** and **10** are quite reasonable in view of the literature data²⁴ for μ_3 -oxo-bridged $\text{Fe}^{\text{III}}_3\text{O}$ complexes. Almost all of the triangular $\text{Fe}^{\text{III}}_3\text{O}$ complexes which have been studied have the same (carboxylate) bridging groups for all three sides of the triangle, *i.e.*, they have the composition of $[\text{Fe}_3\text{O}(\text{O}_2\text{CR})_6\text{L}_3]^+$. The crystal site symmetries, however, are lower than C_3 for the $\text{Fe}^{\text{III}}_3\text{O}$ complexes for which X-ray structures have been reported.²⁴ Thus, the variable-temperature magnetic susceptibility data for several of these complexes have been fit using two exchange parameters ($J_1 = J_2$ and J_3). There is only one well-studied asymmetric $\text{Fe}^{\text{III}}_3\text{O}$ complex, $[\text{Fe}_3\text{O}(\text{TIEO})_2(\text{O}_2\text{CPh})_2\text{Cl}_3] \cdot 2\text{C}_6\text{H}_6$, where the ligand TIEOH has the structure shown below. The $\text{Fe}^{\text{III}}_3\text{O}$ triangle is clearly isosceles. Gorun *et al.*²⁵ fit the susceptibility data for this complex to find $J_1 = J_2 = -8.0 \text{ cm}^{-1}$ and $J_3 = -55 \text{ cm}^{-1}$. This corresponds to an $S_T = 5/2$ ground state. All of the J values are in the range of those evaluated in our theoretical fits of the data for the two Fe^{III}_6 complexes.



Conclusion

The syntheses and X-ray structures of two new hexanuclear ferric complexes, **9** and **10**, have been reported. Both of these complexes consist of two μ_3 -oxo Fe^{III}_3 triangular complexes bridged together at two vertices. Fitting of variable-field magnetization data shows that complex **9** has an $S_T = 5$ ground state. Since pairwise magnetic exchange interactions between high-spin Fe^{III} ions are invariably antiferromagnetic, the $S_T = 5$ ground state results from spin frustration.

All of the spins in each Fe_3O triangle which make up complex **9** would prefer to pair up to give an $S_T = 0$ triangular unit. However, because of the topology of the Fe_3O unit and the competition between the two or three different pairwise exchange interactions in each Fe_3O unit, the spins on certain Fe^{III} ions cannot totally pair up. For an isosceles $\text{Fe}^{\text{III}}_3\text{O}$ triangular complex where $J_1 = J_2 \neq J_3$ we have shown⁷ in detail that spin frustration

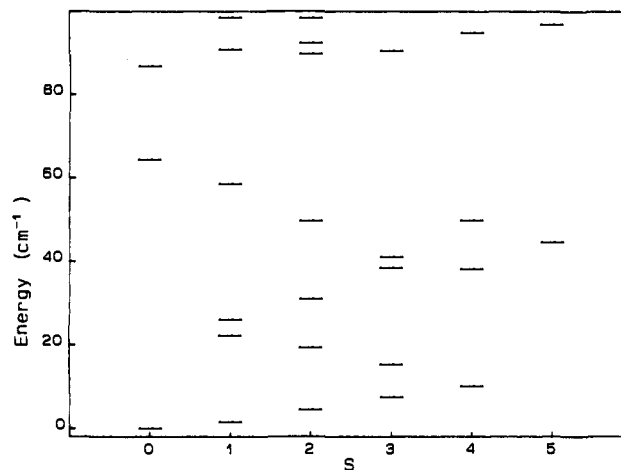


Figure 10. Calculated energies of the spin states lying within 100 cm^{-1} of the $S_T = 0$ ground state of $[\text{Fe}_6\text{O}_2(\text{C}_6\text{H}_5\text{NO})_8\text{Cl}_4](\text{ClO}_4)_2 \cdot \text{MeCN}$ (**10**·MeCN) assuming $J_1 = J_2 = -18(1) \text{ cm}^{-1}$, $J_3 = -52(2) \text{ cm}^{-1}$, and $J_4 = -3(2) \text{ cm}^{-1}$.

is present, and that only small changes in the J_1/J_3 ratio are needed to change the spin of the ground state in such a complex. The ground state can have an S_T value of $1/2$, $3/2$, or $5/2$, depending on the J_1/J_3 ratio. Thus, for complex **9** each of the two $\text{Fe}^{\text{III}}_3\text{O}$ triangular complexes probably has $S_T = 5/2$. Furthermore, the two $\text{Fe}^{\text{III}}_3\text{O}$ triangles are bridged together to form complex **9** in such a way that there is likely spin frustration in the whole Fe^{III}_6 complex. The 10-unpaired-electron ground state in complex **9** does not result from a ferromagnetic interaction between the two $S_T = 5/2$ $\text{Fe}^{\text{III}}_3\text{O}$ triangular subunits.

The spin frustration present in Fe^{III}_6 complex **10** is different than that present in complex **9** or isostructural complex **5**. From fitting variable-field magnetization data for complex **10** it is possible to conclude that in a magnetic field it has a ground state either with $S_T = 3$ or a thermal average over several states where the average has an "effective" $S_T = 3$.

The results of theoretical calculations of the spin-state orderings are reported for complexes **5** and **10**. Good fits of the 10.0-kG data for both of these complexes in the 20–320 K range are given. Thus, even though these Fe^{III}_6 complexes have 4332 different spin states, it has been shown possible to fit the susceptibility data for these complexes by employing irreducible tensorial techniques. This is significant, for now experimental and theoretical techniques can be combined to tune the spin of the ground state of polynuclear transition metal complexes.

Acknowledgment. We are grateful for support from the National Institutes of Health (Grant No. HL13652 to D.N.H. and Grant No. GM 39972 to D.F.H.), the National Science Foundation (Grant No. CHE-9115286 to D.N.H.), the American Cancer Society (Junior Faculty Research Award to D.F.H.), and the Alfred P. Sloan Foundation (Sloan Award to D.F.H.). We thank A. K. Powell for providing coordinate data for complex **8**.

Supplementary Material Available: Tables of atomic positional parameters, complete bond lengths and bond angles, anisotropic thermal parameters, calculated hydrogen atom positions, and magnetic susceptibility data for complexes **9**· $4\text{CH}_2\text{Cl}_2$ and **10**· 4MeCN (16 pages); listings of observed and calculated structure factors for both complexes (39 pages). This material is contained in many libraries on microfiche, immediately follows this article in the microfilm version of the journal, and can be ordered from the ACS; see any current masthead page for ordering information.

(24) Cannon, R. D.; White, R. P. *Prog. Inorg. Chem.* **1988**, *36*, 195.

(25) Gorun, S. G.; Papaefthymiou, G. C.; Frankel, R. B.; Lippard, S. J. *J. Am. Chem. Soc.* **1987**, *109*, 4244.